Journal of Operation and Automation in Power Engineering
Vol. 6, No. 1, Jun. 2018, Pages: 13-22
http://joape.uma.ac.ir

An Intelligent Method Based on WNN for Estimating Voltage Harmonic Waveforms of Non-Monitored Sensitive Loads in Distribution Network

A. Deihimi [*], *A. Rahmani*

Bu-Ali Sina University, Department of Electrical Engineering, Shahid Fahmideh Street, 6517838683 Hamedan, Iran

Abstract- *An intelligent method based on wavelet neural network (WNN) is presented in this study to estimate voltage harmonic distortion waveforms at a non-monitored sensitive load. Voltage harmonics are considered as the main type of waveform distortion in the power quality approach. To detect and analyze voltage harmonics, it is not economical to install power quality monitors (PQMs) at all buses. The cost associated with the monitoring procedure can be reduced by optimizing the number of PQMs to be installed. The main aim of this paper is to further reduce the number of PQMs through recently proposed optimum allocation approaches. An estimator based on WNN is presented in this study to estimate voltage-harmonic waveforms at a non-monitored sensitive load using current and voltage at a monitored location. Since capacitors and distributed generations (DGs) have a special role in distribution networks, they are considered in this paper and their effects on the harmonic voltage waveform estimator are evaluated. The proposed technique is examined on the IEEE 37-bus network. Results indicate the acceptable high accuracy of the WNN estimator.*

Keyword: Distributed network, Power quality monitoring, Voltage harmonic, Wavelet neural network.

1. INTRODUCTION

Sensitive equipment such as electronic devices, which is now more interconnected in distribution networks and industrial processes, can fail or malfunction if subjected to a power quality (PQ) problem. One of the main concerns of power quality is harmonics. Harmonics result in an increased audible noise from motors and transformers, while harmonic voltage and current cause false trip-ping of ground fault interrupters [1]. The monitoring of power system identifies the PQ problems. PQ monitoring is often done to improve the system-wide PQ performance. In conventional PQ monitoring methods, monitors are installed at all the buses in a power distribution network to monitor PQ events. But reducing the number of monitors caused to reduce the total cost of monitoring systems, besides reducing redundancy of data being measured by monitors. New methods are required for selecting the minimum number and the best locations of monitors to reduce monitoring costs without missing essential waveform information [2–9].

Received: 22 Apr. 2017
Revised: 20 Jun. 2017
Accepted: 08 Aug. 2017
∗Corresponding author:
E-mail: a.deihimii@basu.ac.ir (A.Deihimi)
Digital object identifier: 10.22098/joape.2018.3533.1280

A hidden Markov model was developed to classify power quality disturbances in [2]; similarly [3] presents a method to determine the optimal number and placement of PQMs in power systems by using genetic algorithm (GA) and Mallow's Cp . Recent study [4] uses genetic algorithm to estimate the harmonic states of the power network. The methodology was shown to be effective for estimating voltage and current state variables. Reference [5] proposed a transient state estimator to detect losses due to poor PQ. The estimator was validated on a test system to detect the presence of voltage sag. Another estimator was proposed in [6] that improves the power consistency by identifying angle biases and current scaling errors using phasor-measurement-based state estimator. In [7] a novel adaptive quantum-inspired binary gravitational search algorithm is proposed to solve the optimal PQ monitor placement problem in power systems. In [8] a monitor positioning algorithm based on graph theory was developed to determine the optimal number and locations of PQMs in distribution system. In this algorithm system topology is considered to form the coverage matrix. Wavelet transform-based optimal PQ monitoring location was developed in [9]. Reference [10] proposes the voltage-sag waveform estimator as a virtual voltage-sag monitor for online remote estimation of voltage-sag waveforms. The optimal trade-offs between deployment of smart metering devices and phasor

measurement units for distribution system state estimation, meeting the state estimation accuracy limits at the lowest possible cost, is studied in [11,12]. Several methods have been proposed to identify harmonic current such as the methods based on the FFT in frequency domain and the methods based on instantaneous power calculation in time domain [13]. The concept of artificial neural networks, such as echo state networks [14] and adaptive wavelet neural networks [15], has been introduced for the detection of harmonics amplitude. But effects of load currents and voltage-harmonic waveform were not considered. These methods may be useful for estimation of harmonics amplitude without any sensitive load.

In this paper, a voltage-harmonic waveform estimator is considered as an integrated part of a PQ monitor located upstream from the sensitive load called virtual voltage-harmonic monitor. PQMs have been installed according to suggestions in [8]. Although each sensitive load needs monitor, the virtual monitor can eliminate this monitor, thereby further reducing the optimum number of PQMs and costs while maintaining essential waveform information. The present study considers the impact of a distributed generation (DG) on distribution networks. DG is assumed in the vicinity of the sensitive load that makes the estimation process more difficult [16]. Specifically, the emerged wavelet neural network (WNN), which takes advantage of the self-learning function of neural networks and the good time-frequency localization characteristics of the wavelet transform function, is more capable of approximation and a better estimation performance [17]. WNN is used here as the voltage-harmonic waveform estimator. Three-phase voltages and currents at a virtual monitor are the input of WNN and three-phase harmonic voltages waveform are its output. The key features of the proposed method include the following: 1) The monitoring costs can be reduced with further reduce of the optimum number of power quality monitors; 2) Sensitive load needs a monitor to determine voltage distortions. This monitor is eliminated and the proposed estimator estimates the voltage harmonic waveforms of sensitive load. 3) Neural estimator based on WNN is considered as an integrated part of a nearest power quality monitor located upstream from the sensitive load.4) With a total of five parameters, namely, input- output layer weights, hidden-to-output layer weights, bias, translation, and dilation, the WNN offers better adaptively; 5) The WNN uses wavelet coefficients; therefore, when compared to the ANN, it provides better harmonic estimates; 6) A simple and reliable back propagation algorithm with adaptive learning rate is used for network parameter training.

2. THE PROPOSED METHOD

In this section, the proposed methodology to use the WNN as an estimator is presented. First, a brief description on principles and training procedure of the WNN is given below.

2.1. Wawelet Neural Network (WNN)

WNNs generally consist of a multilayer feedforward neural network, with one hidden layer, whose transfer functions are drawn from a wavelet basis function. WNNs have a link between network coefficients and the wavelet decomposition to achieve a good approximation quality with a reduced network size [18]. Wavelet decomposition follows a regular grid structure for its parameters; the WNN parameters are adapted from data. Strong self-adaptability, simple network structure, good fault tolerance and non-locality compared with the general feed-forward network and radial basis function network are WNNs advantages. The basic structure of a multiple-input multiple-output WNN is shown in Fig. 1. There are m nodes in the input layer, h nodes in the hidden layer and n nodes in the output layer. where X = (x1, x2, . . . , xm) is the input vector, V = (v1, v2, . . . , vm) is the weight matrix of connections between input layer and hidden layer neurons, W = (w1,w2, . . . ,wh) is the weight matrix of connections between hidden layer and output layer neurons, B = (b1, b2, . . . , bn) is the bias vector of the output layer neurons, and Y = (y1, y2, . . . , yn) is the predicted output vector of WNN. Where ϕ= (ϕ1, ϕ2,…, ϕh) is the output vector of the hidden layer node. The output of WNN can be obtained as:

$$Y = W.\phi^{T} + B \quad (1)$$

The output of hidden layer ϕ can be expressed as:

$$\phi_j = \Psi_j\left(\left(\sum_{i=1}^{m} V_{ij}x_i - d_j\right)/\, a_j\right) \quad j=1{:}\ h \quad (2)$$

where Ψ represents the wavelet basis function, d_j is the translation parameter of the jth wavelon and a_j is the dilation parameter of the jth wavelon. There are many types of wavelets with different shapes and sizes. The selection of a suitable wavelet function is quite critical because the accuracy and efficiency of the WNN greatly depend on it. Among the variety of wavelets, the Morlet wavelet function is commonly used in nonlinear system modeling because it is computationally efficient and differentiable. A Morlet wavelet function can be expressed as:

$$\Psi(x) = \cos(1.75x)\exp\left(-\frac{x^2}{2}\right) \quad (3)$$

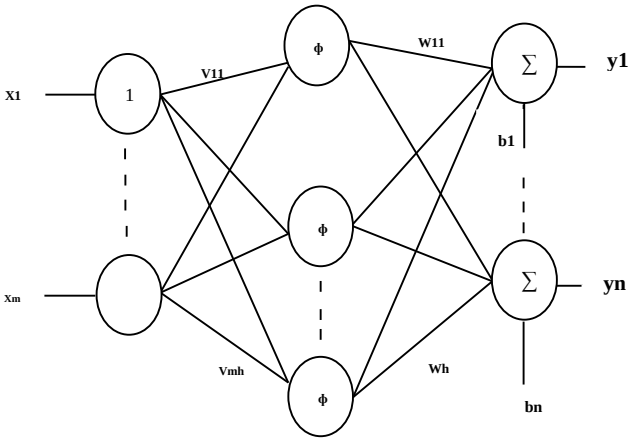

Fig. 1. Basic structure of a multiple-input multiple-output WNN

In this paper, the gradient descent method is used to calculate the network connection weights, by which the parameters in WNN are more accurate than before. Descent method is simple and able to update each parameter simultaneously. However, this method is prone to slow convergence. To counter its slow convergence rate, adaptive learning rate and momentum terms are used, which ensures faster learning. The best structure of these parameters should be calculated for minimum error between the estimated and actual values, so mean square error E of WNN is defined as the cost function:

$$E = \frac{1}{2} \times \sum_{k=1}^{n} (y - y_0)^2 \quad (4)$$

where y and y_0 are the desired and actual responses of the nth output neuron, respectively, and n is the number of output neurons. The learning process extends to minimize the cost function.

Network initialization:

The selection of appropriate initial values of learning rate, momentum coefficient, weight, bias, translation and dilation is important. A heuristic initialization method [15] is used in this study. The selection of the number of hidden layers (wavelons) is also important. Few nodes in the hidden layer can prevent convergence, while increasing the number of hidden layers increases the computation complexity. A trial-and-error method has been used in this study to find the number of hidden layers. Some of the parameter values used in this study are given in Table 1.

2.2. THE PROPOSED ESTIMATOR

The proposed non-monitored voltage-harmonic waveform estimator (Fig. 2) comprises three WNNs.

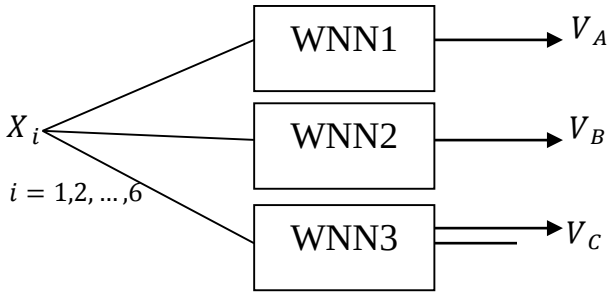

Fig. 2. The proposed method of voltage harmonic waveform estimaton

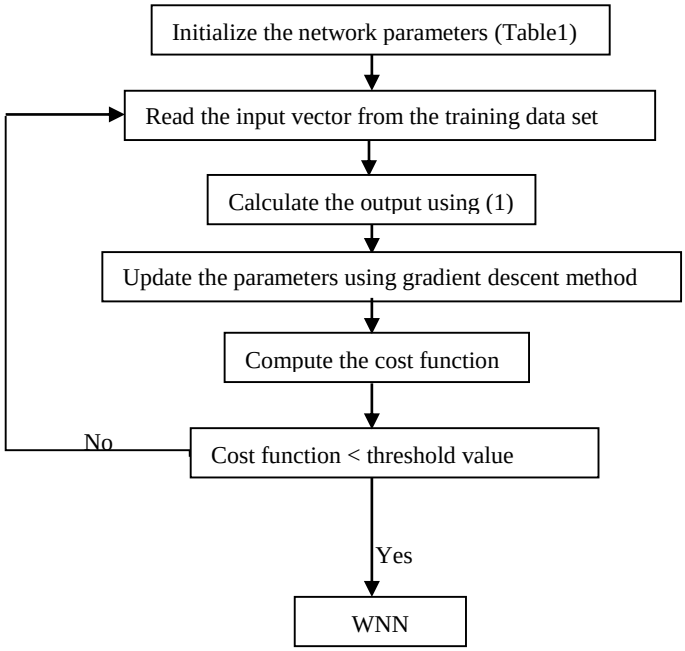

Fig. 3. The proposed WNN-based voltage-harmonic waveform estimation method

Table 1. Parameter values used in the proposed method

Number of input	6	Dilation learning rate	0.2
Number of output	1	Weights learning rate	0.4
Number of hidden layer (wavelons)	200	Bias learning rate	0.01
Threshold cost function	1e-5	Translation momentum coefficient	0.1
Wavelet function	Morlet	Dilation momentum coefficient	0.1
Translation learning rate	0.2	Weights momentum coefficient	0.2
Maximum number of iteration	100	Bias momentum coefficient	0.05

Each WNN has six inputs: locally measured three-phase currents and voltages at the location of the PQ monitor. The single output of each WNN is the voltage of one phase of the sensitive load. Where X_i is the voltage

and current at the monitored bus 37: ($X_1 = V_{AM}$, $X_2 = V_{BM}$, $X_3 = V_{CM}$,$X_4 = I_{AM}$, $X_5 = I_{BM}$, $X_6 = I_{CM}$ where subscripts M, A, B, and C represent the measured signals at the monitored locations, Phases A, B, and C, respectively). The WNN is utilized to map the relationships between input X_i and output V in order to provide estimates of harmonic-voltage waveforms. The flowchart of the proposed WNN-based voltage-harmonic waveform estimation method is shown in Fig. 3.

3. THE STUDIED DISTRIBUTION NETWORK

The investigated distribution network is an IEEE-37 bus radial network [19]. The single diagram of this network is illustrated in Fig. 4. This network has 37 buses and 25 loads. The loads are divided into three categories: commercial, residential and industrial types. Simplified version of the profiles shown in Fig. 5. The details of six loading combinations (LC1 to LC6) are given in Table 2. In this work current harmonic sources are selected according to the load profile and simulation done for different harmonic orders [23]. General characteristics of load harmonics and compensated current with three types of modulation systems for pure resistive and inductive loads are presented in [24].

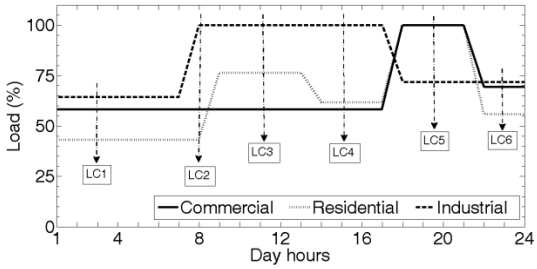

Fig. 5 Simplified version of the load profiles

Table 2. Six different load combinations from simplified hourly load profiles

Load Category	Loading combination					
	LC1	LC2	LC3	LC4	LC5	LC6
Residential (%)	43.27	43.58	76.52	61.87	100	55.8
Commertial(%)	58.3	58.3	58.3	58.3	100	69.53
Industrial (%)	64.35	100	100	100	71.86	71.86

Therefore, in this paper the current harmonic source is assumed as a spectrum with orders 3, 5, 7, 9, and 11 proper to the fundamental component of current corresponding to Table 3 [25, 26].

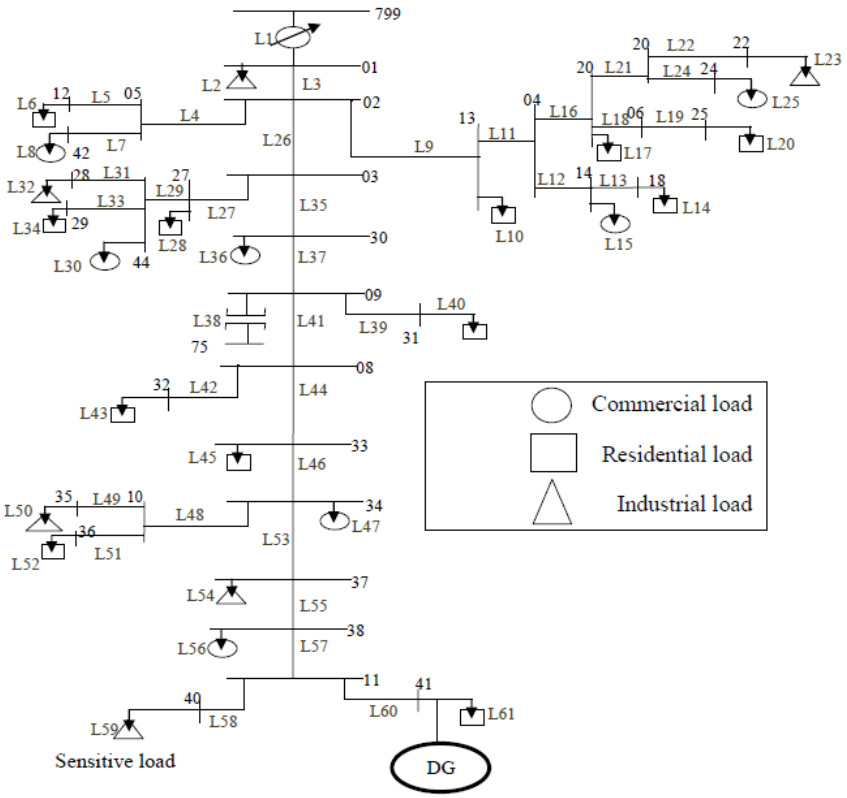

Fig. 4. The IEEE 37-bus distribution network with the sensitive load and a DG

Journal of Operation and Automation in Power Engineering
Vol. 6, No. 1, Jun. 2018, Pages: 13-22
http://joape.uma.ac.ir

Table 3. Harmonic currents as a percentage of the fundamental

Load category	Harmonic current components				
	3	5	7	9	11
Commertial and residential	75	40	13	7	5
Industrial	9	21	10	4	7

An industrial load with high sensitivity to voltage harmonics is assumed at bus 40 as the component L59. A converter-based DG with a gas microturbine system (GMTS) is assumed at bus 41 in the vicinity of the sensitive load. Modelling of the GMTS and connection to the grid are adopted from [10, 20]. On the other hand, it is completely normal that the capacitor bank is used in the power systems network. In this paper it is assumed that a 200-kvar capacitor is located at bus 30 [10] and is used in the grid from 8:15 am to 22:15 pm. So there is a capacitor bank in LC3, LC4, and LC5 profiles. The optimal number of PQMs and the locations on the IEEE-37 bus distribution network are determined in [8]. These results are used here. So, 25 PQMs should be placed at 25 components including L1, L2, L4, L5, L9, L10, L15, L16, L17, L21, L22, L27, L28, L30, L31, L36, L39, L42, L45, L47, L48, L49, L54, L56 and L58. An industrial load with high sensitivity to voltage harmonics is assumed at bus 40 as the component L59. As this load is sensitive, conventionally a monitor is needed to be installed either at its service entrance or at the component L58. This monitor is eliminated in our study, and voltage-harmonic waveform of the sensitive load is estimated by the nearest monitor. For this, the monitor at the component L54 is moved to the component L55 so as to be upstream from the sensitive load. In this paper, the harmonic source is assumed as a current source which injects different orders of the current harmonic component into the power network. The harmonic currents flowing through the system impedance result in harmonic voltages at the load [21, 22].

It is also common to use a single quantity, the total harmonic distortion (THD), as a measure of the effective value of harmonic distortion.

$$THD = \frac{\sqrt{\sum_{h\rangle 1}^{h_{\max}} M_h^2}}{M_1} \quad (5)$$

where Mh is the rms value of harmonic component h of the quantity M.

4. RESULTS AND DISCUSSION

The distribution network and DG system were modeled in Matlab/Simulink on a desktop personal computer (PC) having an Intel Core i5 Duo 2.93-GHz processor and 4-GB random-access memory.

4.1. Simulation method

In this paper, the harmonic source was assumed as a current source. The current distortion for many nonlinear devices is relatively constant and independent of distortion in the supply system. Moreover, the main aim of this research is to estimate the harmonic voltage waveform at a non-monitored sensitive load. The affectivity of the harmonic component orders of more than 11 is negligible. Thus, in this paper, orders lower than 11 were assumed. According to the investigated systems topology, the changes that may occur are as follows: to be or not to be the capacitor, the DG, loads, and lines. Harmonic source location can be determined with reference to harmonic intensity and THD difference between the monitored bus and sensitive load. It is important for the voltage-harmonic waveform estimator to discriminate between different effects of three kinds of harmonic distortion—one set containing all harmonic distortion in the area extended from the sensitive load to the voltage-harmonic waveform estimator including the DG in vicinity of the sensitive load, called here virtual monitoring area (VMA), and the second set comprising all harmonic distortions outside the VMA, and the last kind is harmonic pollution at a sensitive load. The VMA contains the bus whose measured voltages and currents are inputs to the voltage-harmonic waveform estimator. Owing to their direct effects, all the buses in the VMA are important for to be considered as harmonic source location in simulations.

To reduce the number of simulations for harmonic source location outside the virtual monitoring area, a large number of trends of voltage THD variations at buses 37 and 40 were evaluated under different conditions. Typical results are only presented here to show how the final harmonic source location selections are achieved. The THD difference between buses 40 and 37 varied in a certain range due to harmonic source location in different load demands, harmonic orders, and network topologies. The final selection of harmonic source location is achieved by a proper interpolation from the curve of THD difference between buses 40 and 37. Fig. 6 demonstrates voltage THD magnitudes at buses 37

and 40, as well as their THD differences which were evaluated for the current seventh harmonic source at each bus for LC4 including capacitor, all loads, lines, and DG. Besides, Fig. 7 shows the above result and condition, without DG. For the case with DG, the seventh harmonic source outside the VMA and non-zero voltage THD differences, only few buses including buses 01 and 35 could be selected by proper interpolations for the results of other locations as shown in Fig. 6. For the case without DG as shown in Fig. 7, the THD difference outside the VMA was zero.

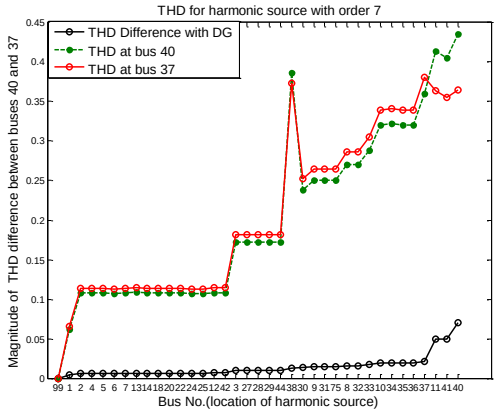

Fig. 6 Effects of locations of harmonic source on voltage THD magnitudes at buses 37 and 40 and their difference for LC4 (with DG)

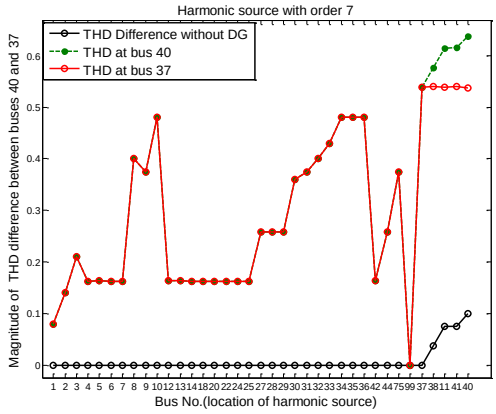

Fig. 7 Effects of locations of harmonic source on Voltage THD magnitudes at buses 37 and 40 and their difference for LC4 (without DG)

Therefore, the selected number of buses can be even fewer, e.g. two buses. After the evaluation and investigation of a large number of voltage THD difference trends, the final selection includes buses 01, 08, 12, 13, and 35 as current harmonic source locations outside the VMA for cases with DG and without DG. It is noted that the buses inside the VMA are also considered harmonic source locations for simulations. However, bus 40 is ignored because this bus is the location of sensitive load and should be prevented from any harmonic distortion.

The current harmonic sources were placed at buses 01, 08, 12, 13, 35, 41, 11, 37, and 38 inject harmonic distortion with orders 3, 5, 7, 9, and 11. Figure. 8 illustrates voltage THD difference between monitored and non- monitored buses (37, 40) for load profiles LC1 to LC6 (a 200-kvar capacitor is considered at LC3, LC4, and LC5 profiles). It must be noted that, in Fig. 8, the voltage THD difference profile is located between those of LC4 and LC5for LC3, and between those of LC1 and LC2for LC6. Therefore, according to the interpolation concept, the voltage THD difference curve for LC3 and LC6 can be attained from other profiles.

Considering the above points, current harmonic sources were placed at buses 01, 08, 12, 13, 35, 41, 11, 37, and 38, and load profiles at LC1, LC2, LC4, and LC5, i.e. two without the capacitor and two with the capacitor. The waveforms of currents and voltages at the bus 37 and voltages at the bus 40 were collected for the purpose of training, validating and testing the WNN.

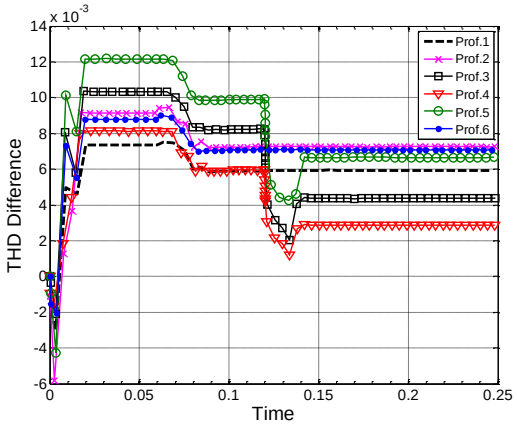

Fig. 8 Voltage THD difference profiles for LC1-LC6 at buses 37 and 40 for the described harmonic spectrum

4.2. Testing the proposed estimator

For the purpose of training, validating and testing the WNN, the currents and voltage waveforms at the monitored bus (L55) and voltage waveforms at the non-monitored sensitive load (L59) of the nominal frequency of 60 Hz were collected with the sampling frequency of 3 kHz. 80% of the data is used for training and validation purposes while the rest is used for testing. For purposes of evaluation, the proposed method's minimum square error MSE is used:

$$MSE = \frac{1}{n} \times \sum_{k=1}^{n} (y - y_0)^2 \qquad (6)$$

Where y is the desired output, y_0 is the estimated

output; n is the number of data.

In this paper, input data were arranged as an n*6 matrix where matrix columns are phase voltages and current samples at monitored bus 37. Besides, n, the number of matrix row, is the number of simulated data after sampling. The desired output was arranged as an n*3 matrix where matrix columns are phase voltages sampled at non-monitored bus 40. The MSE and mean absolute error (MAE) results of the proposed WNN technique for test signals are given in Table 4. MAE can be expressed as:

$$MAE = \frac{1}{n}\sum_{k=1}^{n}|y - y_o| \quad (7)$$

Also, the proposed wavelet neural network is tested in buses 10, 24, 29. We assume the nearest PQ monitor to these buses are placed at buses 34, 20 and 3 respectively. For training and testing purposes, voltages and currents of the monitor location and voltages of buses 10, 24, 29 are collected. The total numbers of each signal is 200. These 200 signals are divided into two sets for training and testing purposes. The MSE results of the proposed WNN technique for estimation of harmonic voltage waveform of buses 10, 24, 29 are given in Table 5.

Moreover, the actual and estimated voltages of sensitive load are presented in Figs. 9–10 for further comparisons:

Assuming the LC1 profile (without DG) with the sustained disconnection of the lines L4, L9 and L7, three phase harmonic source, comparison between estimated and actual voltages of phase a is depicted in Fig. 9(a). In this case MSE is $6.873*e^{-4}$. Figure. 9(b) illustrates the error. For further comparisons, Fig. 9(c) shows the enlarged phase a voltage-harmonic waveform.

Assuming the LC4 profile (with DG) with the sustained disconnection of the lines L7, L9 and load L45, the single-phase harmonic source, estimated and actual voltages of phase a are depicted in Fig. 10(a). Fig. 10(b) shows the enlarged phase a voltage-harmonic waveform with depicted high accuracy of the estimated waveform, in this case MSE is $1.1579*e^{-5}$.

Assuming the LC4 profile (with DG) with the sustained disconnection of the lines L27, L9 and load L30, the two-phase harmonic source, comparison between estimated and actual voltages of phase a are depicted in Fig. 11(a). In this case MSE is $1.3040*e^{-5}$. For more comparison, Fig. 11(b) shows the enlarged phase a voltage-harmonic waveform and Fig. 11(c) illustrates the error.

Assuming the LC5 profile (with DG) with the sustained disconnection of the lines L9, L29 and L48, two-phases harmonic source, estimated and actual voltages of phase a is depicted in Fig. 12 (a), also Figs. 12(b) and 12(c), show enlarged phase a voltage-harmonic waveform and estimated error. In this case MSE is $3.1104*e^{-5}$.

Table 4. MSE and MAE evaluated for the proposed WNN-based voltage-harmonic waveform estimation method

Training MSE error	Training MAE error	Test MSE error	Test MAE error
2.6683e-006	0.0011	0.0067	0.0169

Table 5. MSE evaluated for estimation of harmonic voltage waveform of buses 10, 24, 29

Bus no.	Training MSE error	Test MSE error
10	1.9582e-006	0.0096
24	2.7951e-006	0.0091
29	2.9911e-006	0.0084

Multilayer perceptron neural network (MLPNN) and radial basis function neural network (RBFNN) were trained, validated and tested with the same training, validating and testing data sets of this study. The numbers of hidden layer neurons in the case of RBFNN and MLPNN were respectively 200 and 250. The MSE values of training and validating are 0.0011, and for testing the value is 0.0761 for MLPN. MSE values of training and validating are 6.02e-4, and for testing the value is 0.0541 for RBFNN. Obviously, the ESNs present more accurate estimations.

5. CONCLUSIONS

To further reduce the number of PQMs, an intelligent method based on WNN model was proposed in this paper as a virtual voltage-harmonic monitor for the estimation of voltage harmonic waveforms at a non-monitored sensitive load with a grid-connected DG in its vicinity. The estimator is considered as an integrated part of a PQ monitor placed at another component of the distribution network upstream from and near the sensitive load. The proposed method was examined on the IEEE 37-bus network and showed a high accuracy of estimations. Thus, using the proposed method, the optimal number of PQMs where obtained by recently proposed approaches will be reduced.

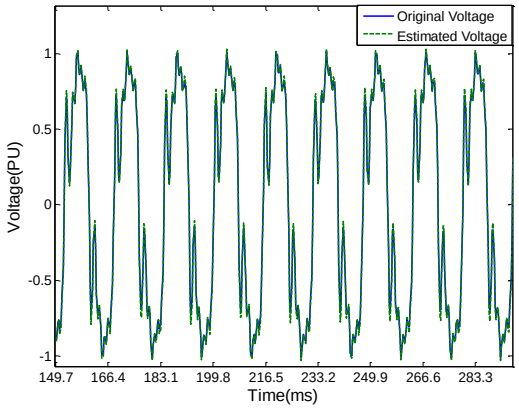

(a)

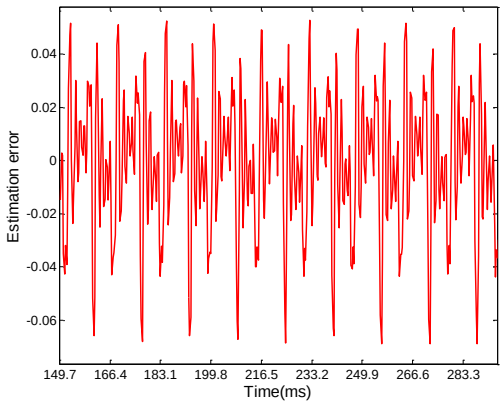

(b)

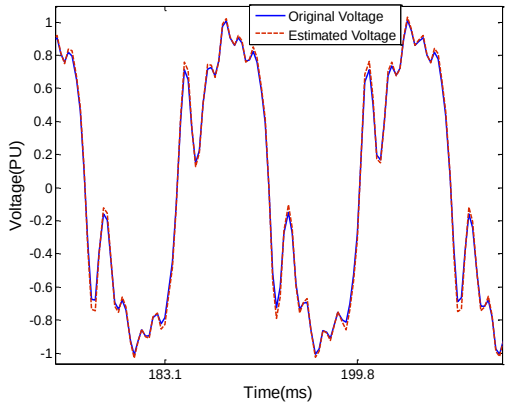

(c)

Fig. 9 Waveforms for simulation result of one test sample: (a) comparison between estimated and actual sampled voltages of phase A, (b) estimation error, (c), enlarged phase A voltage harmonic waveform

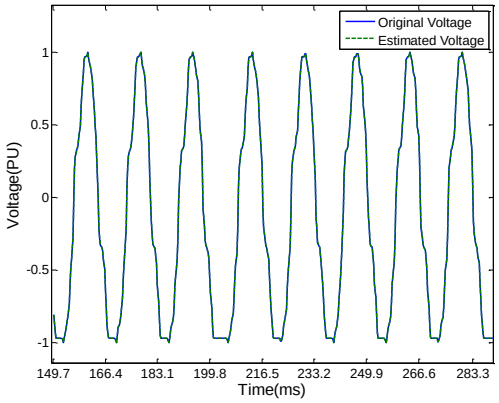

(a)

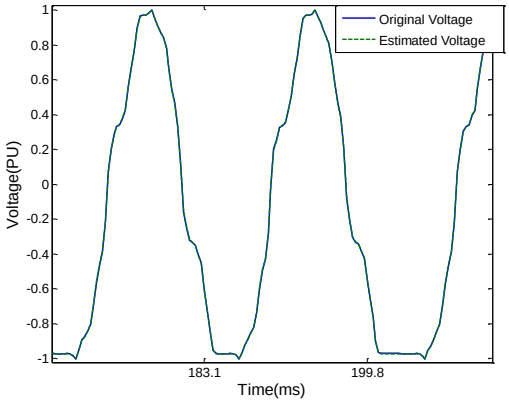

(b)

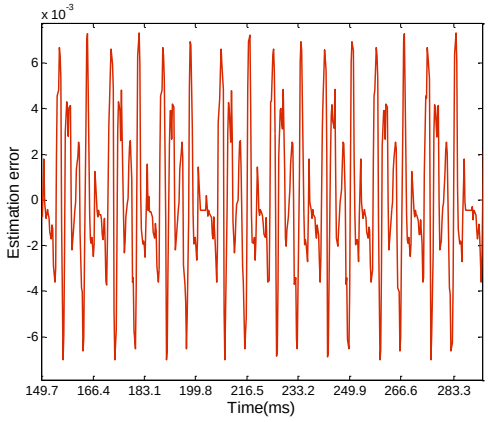

(c)

Fig. 10 Waveforms for simulation result of one test sample: (a) comparison between estimated and actual sampled voltages of phase A, (b) enlarged phase A voltage harmonic waveform, (c) estimation error.

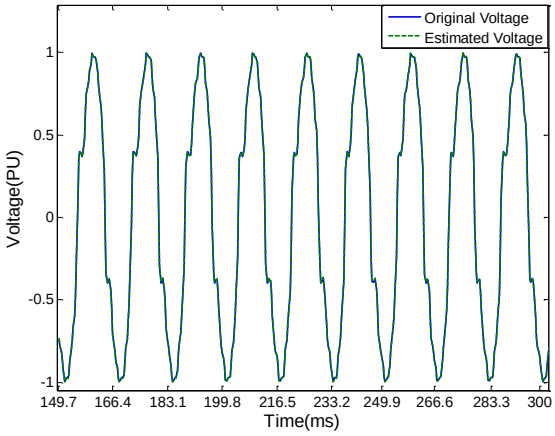

(a)

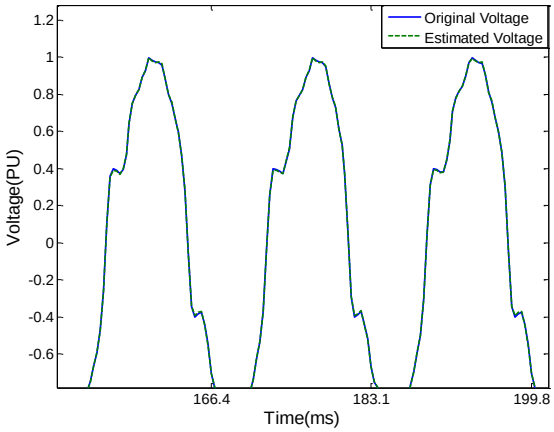

(b)

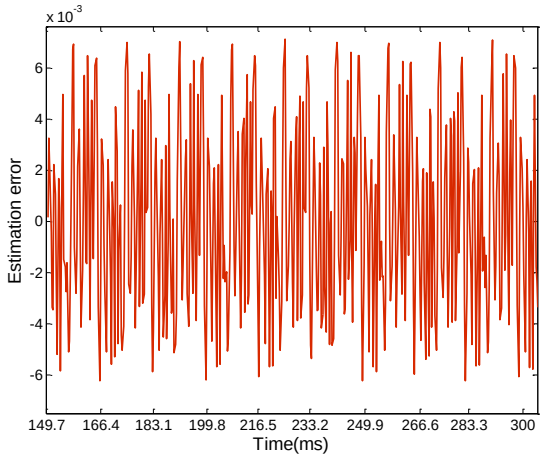

(c)

Fig. 11 Waveforms for simulation result of one test sample: (a) comparison between estimated and actual sampled voltages of phase A, (b) enlarged phase A voltage harmonic waveform, (c) estimation error.

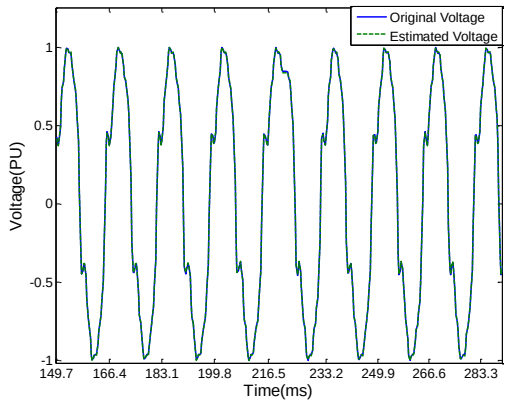

(a)

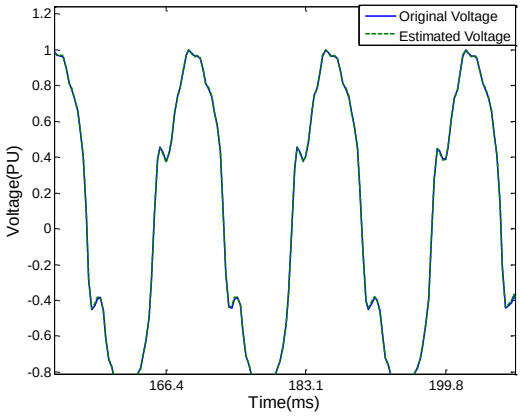

(b)

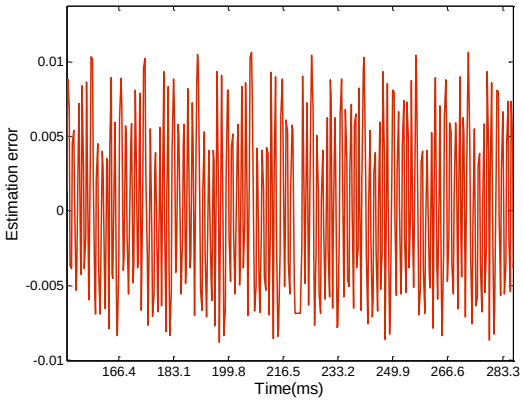

(c)

Fig. 12 Waveforms for simulation result of one test sample: (a) comparison between estimated and actual sampled voltages of phase A, (b) enlarged phase A voltage harmonic waveform, (c) estimation error.

REFERENCES

[1] A. Kusko, M.T. Thompson, "Power Quality in Electrical Systems," McGraw-Hill, 2007.

[2] H. Dehghani, B. Vahidi, R. Naghizadeh, S.H. Hosseinian, "Power quality disturbance classification using a statistical and wavelet-based hidden Markov model with Dempster-Shafer algorithm," *Electr. Power Energy Syst.*, vol. 47, pp. 368-377, 2013.

[3] A. Kazemi, A. Mohamed, H. Shareef, H. Zayandehroodi, "Optimal power quality monitor placement using genetic algorithm and Mallow's Cp," *Electr. Power Energy Syst.*, vol. 53, pp. 564-575, 2013.

[4] C. F. M. Almeida and N. Kagan, "Harmonic state estimation through optimal monitoring systems," *IEEE Trans. Smart Grid.*, vol. 4, no. 1, pp. 467-478, 2013.

[5] A. Farzanehrafat, N. R. Watson, "Power quality state estimator for smart distribution grids," *IEEE Trans. Power Syst.*, vol. 28, no. 3, pp. 2183-2191, 2013.

[6] S. G. Ghiocel, J. H. Chow, G. Stefopoulos, B. Fardanesh, D. Maragal, B. Blanchard, M. Razanousky, and D. B. Bertagnolli, "Phasor-measurement-based state estimation for synchrophasor data quality improvement and power transfer interface monitoring," *IEEE Trans. Power Syst.*, vol. 29, no. 2, pp. 881-888, 2014.

[7] E. Rashedi, H. Nezamabadi-pour, S. Saryazdi, "GSA: a gravitational search algorithm," *Inform. Sci.*, vol. 179, no. 13, pp. 2232-2248, 2009.

[8] D.J. Won, S.I. Moon, "Optimal number and locations of power quality monitors considering system topology," *IEEE Trans. Power Delivery*, vol. 23, pp. 288-295, 2008.

[9] Y.Y. Hong, Y.Y. Chen, "Placement of power quality monitors using enhanced genetic algorithm and wavelet transform," *IET Gener. Transm. Distrib.*, vol. 5, pp. 461-466, 2011.

[10] A. Deihimi, A. Momeni, "Neural estimation of voltage-sag waveforms of non-monitored sensitive loads at monitored locations in distribution networks considering DGs," *Electr. Power Syst. Res.*, vol. 92, pp. 123-137, 2012.

[11] J. Liu, F. Ponci, A. Monti, C. Muscas, P. A. Pegoraro, and S. Sulis, "Optimal meter placement for robust measurement systems in active distribution grids," *IEEE Trans. Instrum. Meas.*, vol. 63, no. 5, pp. 1096-1105, 2014.

[12] M. G. Damavandi, V. Krishnamurthy, and J. R. Martí, "Robust meter placement for state estimation in active distribution systems," *IEEE Trans. Smart Grid*, vol. 6, no. 4, pp.1972-1982, 2015.

[13] R. Kazemzadeh, E. Najafi Aghdam, M. Fallah, Y. Hashemi, "Performance scrutiny of two control schemes based on DSM and HB in active power filter," *J. Oper. Autom. Power Eng.*, vol. 2, no. 2, pp. 103-112, 2014.

[14] A. Deihimi, A. Rahmani, "Application of echo state network for harmonic detection in distribution networks," *IET Genera. Transm. Distrib.*, vol. 11, no. 5, pp. 1094-1101, 2017.

[15] S.K. Jain, S. N. Singh, "Low-order dominant harmonic estimation using adaptive wavelet neural network," *IEEE Trans. Ind. Electron.*, vol. 61, pp. 428-435, 2014.

[16] B. Renders, K. D. Gussemé, W.R. Ryckaert, K. Stockman, L. Vandevelde, M.H.J. Bollen, "Distributed generation for mitigating voltage dips in low-voltage distribution grids," *IEEE Trans. Power Delivery*, vol. 23, pp. 1581-1588, 2008.

[17] R. Song, "Multiple attribute decision making method andapplication based on wavelet neural network," *Control Decis.*, vol. 15, no. 6, pp. 765-768, 2000.

[18] Q. Zhang, A. Benveniste, "Wavelet networks," *IEEE Trans. Neural Netw.*, vol. 3, no. 6, pp. 889-898, 1992.

[19] W.H. Kersting, "Radial distribution test feeders," IEEE/PES., Winter Meeting, 2001.

[20] A. Bertani, C. Bossi, F. Fornari, S. Massucco, S. Spelta, F. Tivegna, "A micro turbine generation system for grid connected and islanding operation," IEEE PSCE., New York, 2004.

[21] R.C. Dugan, M.F. McGranaghan, S. Santo, H.W. Beaty, "Electrical Power System Quality," 2nd Ed., McGraw-Hill, New York, 2003.

[22] J.S. LAI, T.S. KEY, "Effectiveness of harmonic mitigation equipment for commercial office buildings," *IEEE Trans. Ind. Appl.*, vol. 33, pp. 1065-1110, 1997.

[23] N.R. Watson, "Power quality state estimation," *Eur. Trans. Electr. Power*, vol. 20, pp. 19-33, 2010.

[24] B. Mohammadi, A. Mokari, H. Seyedi, S. Ghasemzadeh, "An improved under-frequency load shedding scheme in distribution networks with distributed generation," *J. Oper. Autom. Power Engin.*, vol. 2, no. 1, pp. 22-31, 2007.

[25] Y.G. Hegazy, M.A. Salama, "Identification the relationship between voltage harmonic distortion and the load of harmonic producing devices in distribution networks," *IEEE Can. Conf. Electr. Comput. Engin.*, pp. 669-674, 1994.

[26] H. E. Mazin, W. Xu, "Determining the harmonic impacts of multiple harmonic-producing loads," *IEEE Trans. Power Delivery*, vol. 26, 1187-1195, 2011.